

Nanoscale

Accepted Manuscript



This is an *Accepted Manuscript*, which has been through the Royal Society of Chemistry peer review process and has been accepted for publication.

Accepted Manuscripts are published online shortly after acceptance, before technical editing, formatting and proof reading. Using this free service, authors can make their results available to the community, in citable form, before we publish the edited article. We will replace this *Accepted Manuscript* with the edited and formatted *Advance Article* as soon as it is available.

You can find more information about *Accepted Manuscripts* in the [Information for Authors](#).

Please note that technical editing may introduce minor changes to the text and/or graphics, which may alter content. The journal's standard [Terms & Conditions](#) and the [Ethical guidelines](#) still apply. In no event shall the Royal Society of Chemistry be held responsible for any errors or omissions in this *Accepted Manuscript* or any consequences arising from the use of any information it contains.



Cite this: DOI: 10.1039/xxxxxxxxxx

Photoluminescence properties of $\text{AgInS}_2\text{-ZnS}$ nanocrystals: the critical role of surface[†]

Théo Chevallier^a, Gilles Le Blevenc^{*a} and Frédéric Chandezon^{b,c,d}Received Date
Accepted Date

DOI: 10.1039/xxxxxxxxxx

www.rsc.org/journalname

$\text{AgInS}_2\text{-ZnS}$ (ZAIS) nanocrystals are very good candidates for easily synthesized, highly efficient, cadmium-free nano-phosphors. They can apply for the development of next generation white-LED technologies taking advantage of their nanometric size. This paper describes the combined use of time-resolved emission spectroscopy and photoluminescence quantum yield measurements to quantitatively compare the efficiency of each recombination pathway involved in the photoluminescence of ZAIS nanocrystals. This approach, applied on nanocrystals of different size, composition and surface chemistry revealed the critical role of surface effects. Moreover, we developed a new type of surface passivation that increases the photoluminescence quantum yield of all nanocrystals compositions by 15 to 20%. This molecular surface passivation can be applied in replacement or in addition to the already established ZnS shell passivation method.

1 Introduction

Recent advances in light emitting diodes (LED) led to the great expansion of white-LED (W-LED) devices based on cerium doped aluminum garnet (YAG:Ce) phosphor. Indeed, this phosphor exhibit photoluminescence quantum yields (PLQY) of almost 100% and very good stability regarding aging. On the other hand, the economical stress on rare-earth based phosphors pushed researchers toward highly absorbent semiconductor nanocrystals that could take advantages of nano-optical phenomena.

Cadmium-based luminescent nanocrystals are extensively studied. Their PLQY generally reaches values above 50% in core/shell nanostructures¹. A quantum yield of around 90% was even reported in the case of an hybrid QLED structures². Thanks to extensive research, the photoluminescence of quantum dots is precisely tuned by their size using quantum confinement. However, their toxicity might prevent them from large scale industrial application.

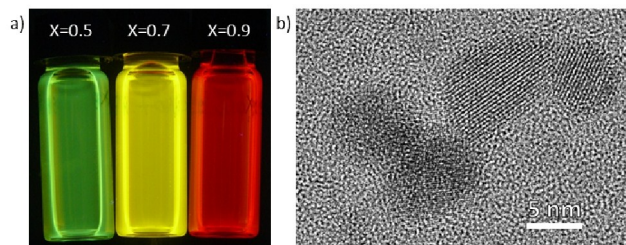


Fig. 1 a) colloidal solutions of $\text{AgInS}_2\text{-ZnS}$ nanocrystals of different compositions observed under UV illumination. b) Typical high resolution TEM image of $\text{AgInS}_2\text{-ZnS}$ nanocrystals ($X=0.7$).

The first alternative to these materials is to use InP-based quantum dots which can reach high quantum yield as well³. Due to the nature of the quantum confinement phenomenon, both these materials require a precise control over the size of the synthesized nanostructures. On the other hand, ternary and quaternary semiconductors nanocrystals based on CuInS_2 and AgInS_2 are another promising alternative for industrial applications⁴ since they do not have that requirement. Indeed, their photoluminescence is easily controlled by their composition using their ability to create solid solutions with zinc sulfide⁵, silver gallium sulfide^{6,7} or copper sulfide⁸. Additionally, their broad luminescence spectrum makes them particularly suitable for the production W-LED devices with a high color rendering index^{9,10}. Their low toxic-

^a CEA, Liten-DTNM, F-38054 Grenoble Cedex 9, France ; Tel: +33 (0) 4 38 78 54 45; E-mail: theo.chevallier@gmail.com

^b Univ. Grenoble Alpes, INAC-SPrAM, F-38054 Grenoble Cedex 9, France

^c CNRS, SPrAM, F-38054 Grenoble Cedex 9, France

^d CEA, INAC-SPrAM, F-38054 Grenoble Cedex 9, France

[†] Electronic Supplementary Information (ESI) available: [details of any supplementary information available should be included here]. See DOI: 10.1039/b000000x/

ity promoted their use in biological applications^{11–14} but ZAIS nanocrystals were also applied in photocatalysis^{15–17}, photodetection¹⁸ and solar cells^{8,19} applications.

Torimoto *et al.* first reported the photoluminescence of AgInS₂–ZnS (ZAIS) solid solutions nanocrystals from the near infrared to green region²⁰ in 2007. Since then, the origin of the broad emission spectrum was shown to be the result of donor-acceptor pair (DAP) recombinations originating from defect states in the band gap^{21–23}. The same team later showed that a heat treatment process and a ZnS shell can substantially increase the quantum efficiency of ZAIS nanocrystals²⁴.

We propose an innovative approach combining the use of time-resolved emission spectroscopy (TRES) and absolute photoluminescence quantum yield measurements to construct and quantitatively compare the emission spectra of each of the luminescence mechanisms. A model is proposed to explain the photoluminescence line-shape of ZAIS nanocrystals. This analysis was carried on nanocrystals of different size, composition and surface chemistry revealing the critical role played by the surface on the efficiency of these materials. A new surface passivation method, more effective and additional to the classical ZnS shell growth, is developed. Using a combination of surface-related improvement strategies, absolute quantum yields of 60–70% and 80% were reached for yellow and red emitting ZAIS nanocrystals respectively.

2 Experimental methods

2.1 Synthesis of AgInS₂–ZnS nanocrystals

The synthesis of AgInS₂–ZnS nanocrystals was based on the method proposed by Torimoto *et al.*²⁰. The precursor (AgIn)_xZn_{2–2x}(S₂CN(C₂H₅)₂)₄ was prepared by precipitation of Ag(NO₃), In(NO₃)₃ and Zn(NO₃)₂ in stoichiometric proportions with an aqueous solution of sodium diethyldithiocarbamate. After washing the powder with water and methanol, 150 mg of the dried precursor were heated at 180°C under argon atmosphere for 30 min. Then, 8 ml of oleylamine were added and the mixture was kept at 180°C during 3 min allowing for the nanocrystals to disperse in oleylamine. Micrometric by-products of the synthesis were eliminated by centrifugation of the solution at 9000 rpm for 10 min. An additional heat treatment process consisting of a 30 min heating of the nanocrystals at 180°C in oleylamine was performed. Nanocrystals were purified from the excess oleylamine

by flocculation and centrifugation in methanol. Finally, they were dispersed in chloroform.

In an alternative process, the dried precursor was directly dispersed in oleylamine. The mixture was then heated up at 180°C for 20 min under argon atmosphere. Purification and dispersion methods were the same as the typical procedure described above.

As shown in figure 1.a), the optical properties of the nanocrystals were primarily controlled by their composition via the composition of the used precursor, itself defined by the parameter X. An X value of 1 indicates the absence of zinc in the structure while an X value of 0 will induce the production of ZnS nanocrystals. More details about the synthesis, size, photoluminescence quantum yield and optical absorption of ZAIS nanocrystals are given as supplementary information†.

2.2 Growth of a ZnS shell

The growth of a ZnS shell onto ZAIS nanocrystals was performed with the nanocrystals dispersed in oleylamine after removal of the synthesis by-products. The dispersion was first heated at 140°C under argon. Then, 15 mg of thioacetamide and 50 mg zinc acetate, both dissolved in 2.5 ml of oleylamine, were added dropwise into the solution. The reaction was kept at 140°C for a total time of 5 min. After cooling down to room temperature, the AgInS₂–ZnS@ZnS core-shell nanocrystals were retrieved by flocculation in methanol and dispersed in chloroform.

2.3 Surface passivation of AgInS₂–ZnS and AgInS₂–ZnS@ZnS nanocrystals

The organic surface passivation of AgInS₂–ZnS and AgInS₂–ZnS@ZnS was performed by adsorbing phosphine-related molecules (typically trioctylphosphine) onto the nanocrystals surface. Typically, 5 μL of trioctylphosphine (TOP) were added to the colloidal solution of nanocrystals in chloroform. A blue-shift and an intensity increase of the photoluminescence spectrum of the colloidal solution are observed. The strong affinity of the phosphine moiety for the ZAIS nanocrystals surface makes the process completed in less than a minute at room temperature. Another proof of the affinity of phosphine-related molecules for the nanocrystals surface is the fact that they can change the nanocrystals colloidal stability. Indeed, the use of small phosphine-related molecules like tributylphosphine or tris(dimethylamino)phosphine quickly destabilizes the colloidal solution in chloroform due to the weaker stabilization they offer compared to oleylamine.

2.4 Characterization techniques

Absolute photoluminescence quantum yield (PLQY) and diffuse absorption spectra of ZAIS nanocrystals colloidal solutions were measured with a Hamamatsu absolute PL quantum yield

† Electronic Supplementary Information (ESI) available: [details of any supplementary information available should be included here]. See DOI: 10.1039/b000000x/
^a CEA, Liten-DTNM, F-38054 Grenoble Cedex 9, France; Tel: +33 (0) 4 38 78 54 45;
E-mail: theo.chevallier@gmail.com

^b Univ. Grenoble Alpes, INAC-SPrAM, F-38054 Grenoble Cedex 9, France

^c CNRS, SPrAM, F-38054 Grenoble Cedex 9, France

^d CEA, INAC-SPrAM, F-38054 Grenoble Cedex 9, France

spectrometer equipped with an integrating sphere (Quantaaurus-QY C11347). Time-resolved emission spectroscopy (TRES) experiments were performed on a Horiba Jobin-Yvon fluorolog-3 spectrometer using a Horiba nanoLED-350 excitation source ($\lambda_{excit} = 350$ nm, pulse time < 1.0 ns). The decay signals were recorded for times between 0 and $7.2 \mu\text{s}$ and integrated until the maximum intensity reached 10^5 counts. A blank measurement allowed for the estimation of the error on the intensity signal.

3 Results and discussion

3.1 Band gap tailing in AgInS_2 -ZnS nanocrystals.

Using a dedicated absolute quantum yield spectrometer, the photoluminescence quantum yield and diffuse absorption of colloidal solutions of ZAIS nanocrystals were measured for excitation wavelengths between 350 nm and 800 nm. For each excitation wavelength, the diffuse absorption of the colloidal solution is measured and therefore a diffuse absorption spectrum is constructed. In the range of sizes and compositions tested in this study, the absorption spectra do not change with respect to the size of the nanocrystals and do not exhibit any excitonic peak, even for narrow size distributions. Quantum confinement therefore does not have any effect on the electronic properties for these sizes and compositions. As already established by Mao *et al.*²⁵, the band gap can be determined using the Tauc law for the band edge absorption of a direct band gap semiconductor^{26,27}:

$$(A \cdot hv) \propto (hv - E_g)^{1/2} \quad \text{for } hv > E_g$$

Where A is the measured diffuse absorption, hv is the energy of the absorbed photons and E_g is the optical band gap of the material[†].

In the case of highly disordered semiconductors, the absorption of photons with energies below the band gap of the material is not negligible. This phenomenon, originating from band gap fluctuations and defects in the crystal structure, is known as "band gap tailing" and is usually modeled, as first proposed by Urbach *et al.*, by the following exponential law²⁸.

$$A \propto \log\left(\frac{hv}{E_u^{Abs}}\right) \quad \text{for } hv < E_g$$

The slope of the $\log(A)$ vs hv curve (for $hv < E_g$) corresponds to the inverse of an energy E_u^{Abs} known as the Urbach energy. A high value of E_u^{Abs} indicates the presence of large structural disorder in the material^{29,30}.

In an effort to understand the parameters influencing the photoluminescence efficiency of ZAIS nanocrystals, we first reproduced the synthesis protocol proposed by Torimoto *et al.*. As described in section 2.1, nanocrystals were synthesized with different composition of starting precursor (X) and underwent a heat treatment process at 180°C for 30 min. The figure 2 presents the photoluminescence quantum yields and Urbach energies for ZAIS

nanocrystals of different compositions, before and after the heat treatment process.

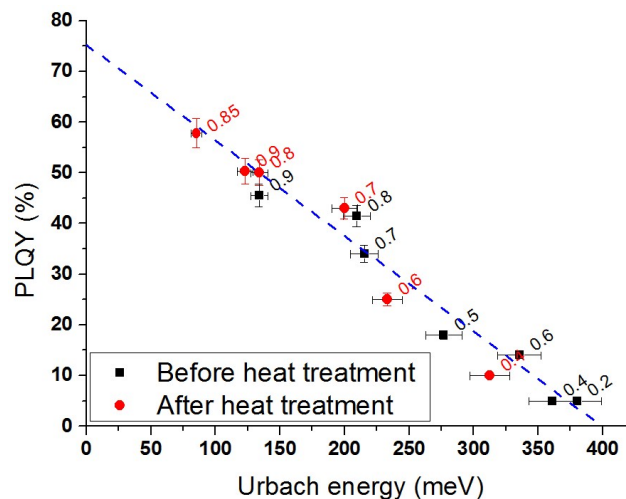


Fig. 2 Photoluminescence quantum yield (PLQY) of AgInS_2 -ZnS (ZAIS) nanocrystals of different composition before and after heat treatment as a function of their Urbach energy. The composition parameter X is indicated for each point.

In the case of ZAIS nanocrystals synthesized with precursor of composition X between 0.4 and 0.9, Urbach energies between 100 meV and 400 meV were measured. Heat treatment of nanocrystals always resulted in a decrease of the Urbach energy associated with an increase of the PLQY. This indicates that the efficiency of ZAIS nanocrystals is hindered by disorder in the structure which is partially reduced by the heat treatment process²⁴. More interestingly, ZAIS nanocrystals of all tested compositions, before or after heat treatment, lie on the same PLQY vs E_u trend curve. This indicates that the evolution of the PLQY of ZAIS nanocrystals with respect to their composition is primarily due to the evolution of the disorder that these compositions induce. Indeed, tetragonal chalcopyrite structures are known to accept important off-stoichiometry⁴.

3.2 Carriers dynamics in ZAIS nanocrystals

In order to differentiate the electronic processes involved in their photoluminescence, the kinetics of ZAIS nanocrystals luminescence were studied using time-resolved emission spectroscopy (TRES). In previous studies^{6,25,31}, the time-resolved intensity signals were fitted with a double-exponential function leading to the assignment of two radiative recombinations pathways associated with donor-acceptor pair (DAP) recombinations from surface and core states respectively.

The quality of a given fitting model is assessed by the visualization of the residual plots and the value of the reduced χ^2 , noted χ_{red}^2 (details in the ESI[†]). In practice, χ_{red}^2 values between

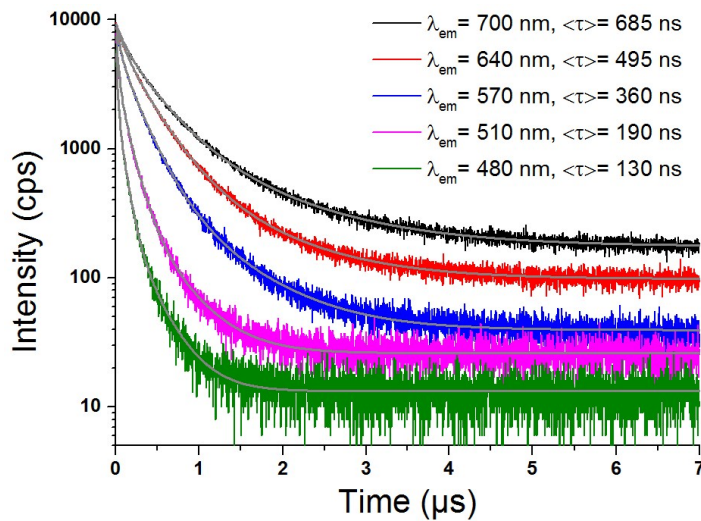


Fig. 3 Example of TRES signals recorded at 5 different wavelengths of the emission spectrum of ZAIS nanocrystals ($X=0.7$) fitted with a 3-exponential function.

0.9 and 1.1 are generally accepted to confirm the relevance of a given fitting model³².

TRES measurements were performed on ZAIS nanocrystals with composition ranging from $X=0.4$ to $X=0.9$ and for emission wavelengths across their emission spectra. All TRES signals were recorded with a 350 nm excitation wavelength since it corresponds to a photon energy above the band gap of all tested compositions. An example of TRES signals recorded for several emission wavelengths is showed in figure 3. Representations in the log-log scale as well as residual plots are presented as supplementary informations. The values of χ_{red}^2 obtained with different fitting models are shown in table 1 along with the probability $P(\chi_{red}^2)$ that such χ_{red}^2 can be obtained because of random errors. It is usually accepted that a model must be rejected if the value of P is smaller than 0.05³².

fitting model	χ_{red}^2	$P(\chi_{red}^2)$
single-exponential	10.0 ± 1.87	$P \ll 0.001$
double-exponential	1.56 ± 0.15	$P < 0.001$
triple-exponential	1.06 ± 0.02	$0.1 < P < 0.2$
quadruple-exponential	1.01 ± 0.02	$0.4 < P < 0.5$
stretched exponential	1.19 ± 0.12	$0.02 < P < 0.05$

Table 1 χ_{red}^2 values obtained with five different models applied on TRES signals recorded for 10 emission wavelengths of ZAIS nanocrystals of composition $X=0.4, 0.7$ and 0.9 . The probability $P(\chi_{red}^2)$ that such χ_{red}^2 value is obtained because of random errors is also presented³³.

When using a double-exponential fitting function, we find that residual plots exhibit large oscillations showing the poor quality of the obtained fit. Moreover, the obtained χ_{red}^2 values indicate

that there is less than a 0.1% chance that the spread of the residuals can be assigned to random error. This model must therefore be rejected. The same observation was made when using a stretched-exponential decay function. Only some of the TRES signals could be satisfactorily explained using this model.

A three-exponential fitting function, however, gives values of χ_{red}^2 between 1 and 1.1 for all tested compositions and emission wavelengths. Although a quadruple-exponential fit gives χ_{red}^2 values closer to the ideal value of 1, this improvement is not sufficient to conclude that the added contribution has any physical meaning. Moreover, the fourth contribution added by this model usually represents a negligible part ($<1\%$) of the total steady-state emission. Therefore, a triple-exponential fit was used for the analysis of the TRES signals recorded with ZAIS nanocrystals.

Fitting the measured TRES signals with the triple-exponential model,

$$I(t, \lambda) = A_1 \cdot e^{-t/\tau_1} + A_2 \cdot e^{-t/\tau_2} + A_3 \cdot e^{-t/\tau_3} + y_0 \quad (1)$$

we determine the photoluminescence lifetimes of each recombination pathway. The proportion of the steady-state photoluminescence intensity produced by a give contribution is also calculated with the formula :

$$\%i(\lambda) = \frac{\int A_i \cdot e^{-t/\tau_i} dt}{\int I(t, \lambda) dt} = \frac{A_i \cdot \tau_i}{\sum_j A_j \tau_j} \quad (2)$$

The figure 4 represents the obtained values for the fluorescence lifetimes and proportions of each contribution in ZAIS nanocrystals of composition $X=0.7$.

These observations are supported by the work of Komarala *et al.* who found the same behavior for $\text{CuInS}_2\text{-ZnS}$ nanocrystals with similar luminescence properties and structure³⁴. Using the order of magnitude of the measured lifetimes, Komarala *et al.* assigned the fastest component (~ 50 ns) to intrinsic radiative recombinations of surface states and the two other components (~ 250 ns and ~ 500 ns) to donor-acceptor pairs recombinations involving surface (DAP_{surf}) and core (DAP_{core}) states respectively. This interpretation completes the interpretation given by Mao *et al.* based on both TRES and time resolved absorption spectroscopy of AgInS_2 nanocrystals²⁵. A representation of these radiative recombination pathways is presented in figure 5. Such interpretation must however be supported by direct experimental data to prove the distinction between core and surface recombination pathways. This is the purpose of the experiments concerning surface modification and size presented in sections 3.4 and 3.5.

In the case of donor acceptor-pair recombinations, the wavelength of the emitted photon resulting from the recombination between carriers in localized donor and acceptor states separated

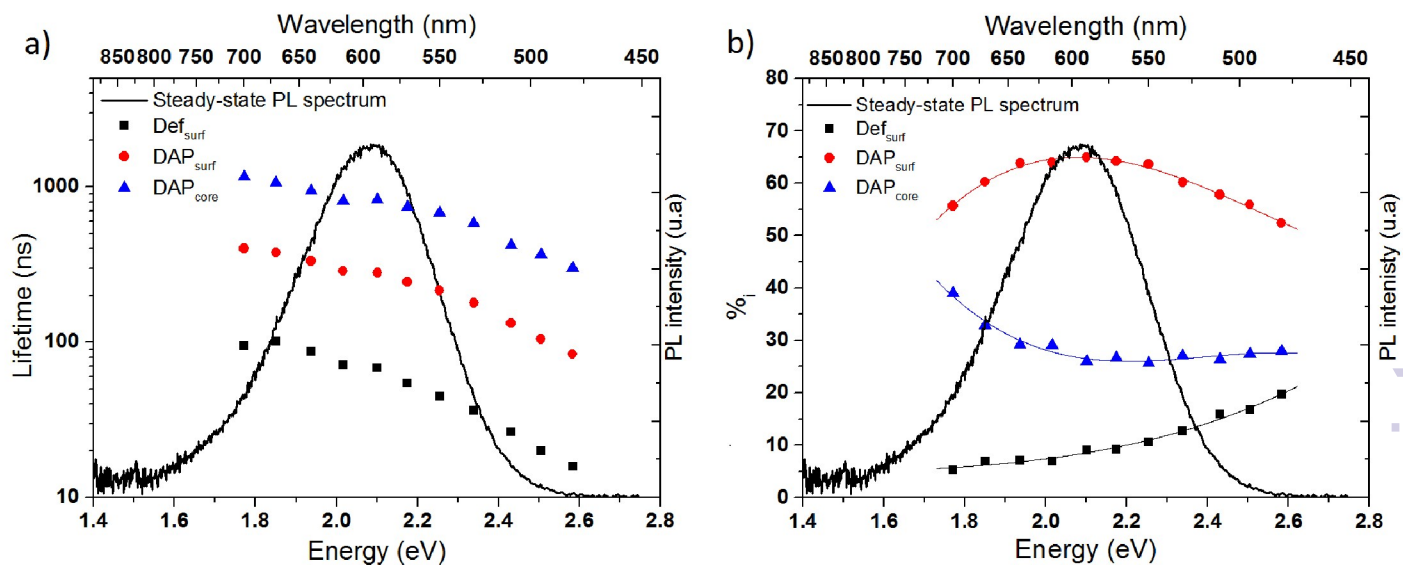


Fig. 4 Example of a) Fluorescence lifetimes and b) proportion of each recombination pathway for emission wavelengths across the emission spectrum of ZAIS nanocrystals (here with $X=0.7$).

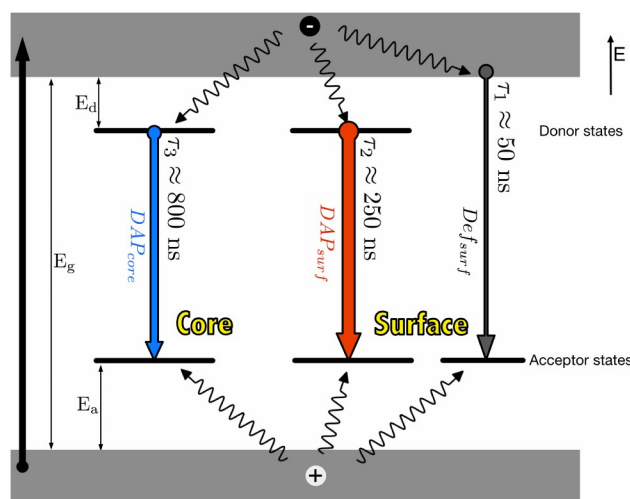


Fig. 5 Photoluminescence mechanisms in AgInS₂-ZnS nanocrystals.

from a distance d in the crystal lattice is :

$$h\nu = E_g - E_d - E_a + \frac{e^2}{\epsilon \cdot d} \quad (3)$$

Where E_g is the band gap of the semiconductor, E_a and E_d are the energy of the acceptor and donor states and ϵ is the permittivity of the material.

Recombinations from distant pairs, leading to the emission of lower energy photons, have a lower probability to occur in a given time than close donor-acceptor pairs. The luminescence lifetime associated with DAP recombinations therefore exponentially in-

creases with the emission wavelength^{35,36}. This effect was clearly observed on all tested ZAIS nanocrystals when performing TRES measurement at different emission wavelengths (see figures 3 and 4.a).

3.3 Photoluminescence line-shape of each emission contribution

In order to observe the evolution of the efficiency of each recombination pathway, we combined the TRES analysis with absolute photoluminescence quantum yield (PLQY) measurements. The photoluminescence quantum yield allows for the quantitative representation of the steady-state emission spectrum. Indeed, after representing the measured steady-state emission spectrum in the energy space using the appropriate Jacobian transformation³⁷, we can normalize the spectrum so that its integral corresponds to the measured PLQY. We therefore effectively created a spectrum representing the probability distribution of emission of photons from the absorption of an exciting photon.

For each wavelength of this steady-state emission spectrum, the TRES analysis presented in section 3.2 allows for the determination of the fraction $\%_i$ of the intensity corresponding to a given contribution "i". Therefore, a quantitative value of the steady-state intensity related to a given recombination pathway can be calculated multiplying the total intensity $I(\lambda)$ by this proportion $\%_i(\lambda)$. By repeating the TRES analysis on several emission wavelengths across the global steady-state emission spectrum, the steady-state emission spectra of each contribution are reconstructed. An example of this analysis is presented in figure 6a. Details about this combined use of PLQY and TRES measure-

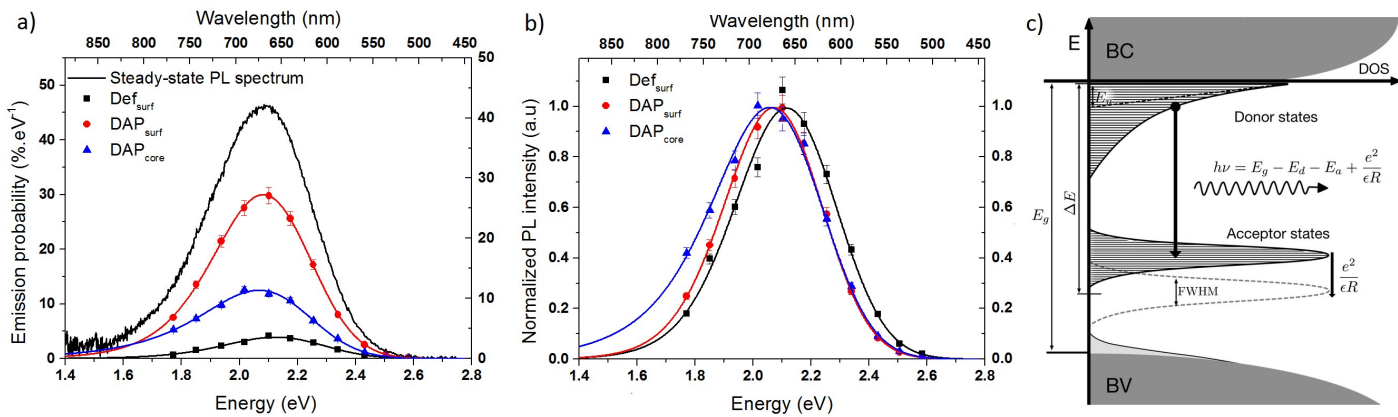


Fig. 6 Example of a combined TRES and PLQY analysis on ZAIS nanocrystals synthesized with a precursor of composition $X=0.7$. a) Measured steady-state PL spectrum ($I_{steady-state}$) and constructed steady-state PL spectra of each contribution (I_i). b) Normalized photoluminescence spectra of each contribution c) Schematic of the model used to fit the photoluminescence line-shape of each contribution's spectrum

ments are presented as supplementary information†.

Having constructed the emission spectra of each of the three emission contributions, we examined these experimental data with theoretical interpretation of photoluminescence line-shape. We found that only the model originally proposed by Ozaki *et al.* for the interpretation of the photoluminescence spectra of AgInSe_2 ³⁸, CdGaTe_2 ³⁹ and ZnIn_2Te_4 ⁴⁰ best fits our data for AgInS_2 - ZnS nanocrystals. This model interprets the spectrum as the convolution product of an exponential and a gaussian functions modeling the density of states of involved donors and acceptors states respectively. The obtained line-shape therefore corresponds to a exponentially-modified gaussian function. The asymmetry and width of this line-shape are respectively linked to the extent of the exponential tail (donor states) and width of the gaussian function (acceptor states) it originates from. The asymmetry of the function has therefore a similar signification as the Urbach energy except that it only considers donor states that are involved in the luminescence process. Both E_u^{PL} and E_u^{Abs} are, in the case of ZAIS nanocrystals, an indirect assessment of the structural disorder. A higher value of E_u^{PL} (i.e. a greater asymmetry) should therefore indicate a lower efficient for the studied luminescent process.

Fitting parameter	DAP _{surf}	DAP _{core}
E_u^{PL} (meV)	125 ± 7	200 ± 20
ΔE (eV)	2.18 ± 0.01	2.19 ± 0.01
FWHM (meV)	338 ± 10	342 ± 10

Table 2 Example of values of the Urbach energy for donor states (E_u), energy position (ΔE) and spread (FWHM) of donor states obtained for the two DAP recombination processes in ZAIS nanocrystals ($X=0.7$).

An exponentially-modified gaussian function was fitted to each spectra corresponding to a particular recombination pathway us-

ing a least squares fitting method. Errors on the intensity of these spectra, mostly originating from the error over the $\%_i$ values, were taken into account in the fitting process in order to estimate the error on the obtained fitting parameters. The Urbach energy obtained via absorption measurements was found to have a similar value as the characteristic energy (E_u^{PL}) of the donor states tail involved in the core recombinations (DAP_{core}). An example of values obtained with this fitting method on the DAP_{surf} and DAP_{core} contributions is given in table 2. As expected by the more asymmetric line-shape of the DAP_{core} contribution spectrum (see figure 6.b), the value of E_u^{PL} associated with donor states is found to be always larger for the DAP_{core} contribution than for the DAP_{surf} contribution. This is also consistent with the fact that surface donor states are, on average, located closer to the conduction band than core donor states as proposed by Mao *et al.*²⁵. These results suggest that surface DAP recombinations are more efficient than core ones. This is reinforced by the fact that about 65% of the total steady-state photoluminescence originates from surface recombination processes while, for this size of nanocrystals, only 30-40% of the atoms are surface atoms. A more direct proof of the better efficiency of surface recombinations will be presented in section 3.5.

The energy distribution of acceptor states, also inferred from the fitting parameters, was found to be the same for both DAP recombination pathways. This suggests that both processes probably involve similar acceptor states. Although it is not possible to conclude on the validity of our fit for the surface states contribution spectrum (Def_{surf}) due to larger measurement errors, it is clear from the figure 6.b that this contribution is blue-shifted from the two others. This is consistent with our attribution of this process to the recombination of carriers from the conduction band to the donor states. These observations were repeated on nanocrystals synthesized with precursors compositions $X=0.4$,

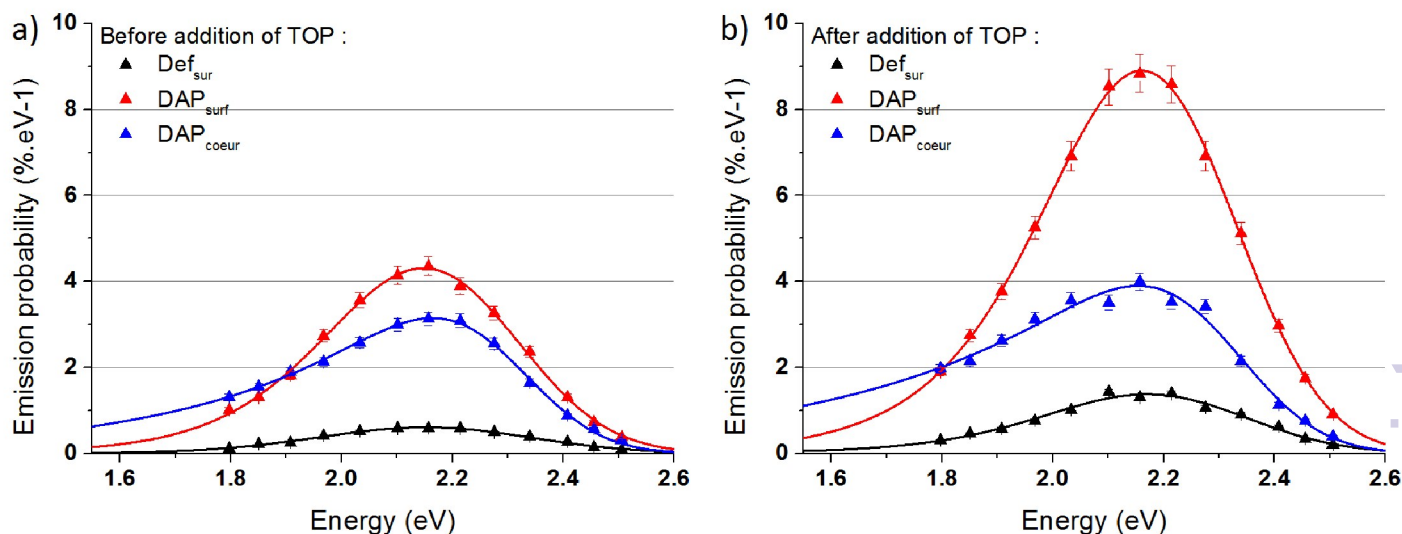


Fig. 7 Effect of the surface passivation by trioctylphosphine on each component of the steady-state emission for ZAIS nanocrystals (here with $X=0.5$).

0.7 and 0.9.

We conclude, as depicted in figure 5, that the photoluminescence of ZAIS nanocrystals is the result of three recombinations pathways involving either surface or core donor states. The emission originating from surface states was found to be more efficient as revealed by its less asymmetric shape and large contribution to the total emission. In the next part, we will further examine the validity of these interpretations by changing the extent and nature of the ZAIS nanocrystals surface. New strategies to improve the photoluminescence quantum yield of ZAIS nanocrystals will be presented and explained in the light of the results presented above.

3.4 The effect of surface passivation.

Surface passivation is known to increase the photoluminescence quantum yield of various luminescent nanocrystals. Torimoto *et al.* were the first to apply this technique on ZAIS nanocrystals. By growing a ZnS shell onto ZAIS nanocrystals, they observed a substantial increase of the photoluminescence quantum yield which they assigned to the passivation of non-radiative surface defects²⁴. Due to the great crystalline structure similarity between cubic ZnS and tetragonal AgInS₂, the ZnS shell easily grows in an epitaxial manner onto the ZAIS nanocrystals surface. However, this similarity also induces a large tendency of ZnS to diffuse into the ZAIS core structure thus modifying the composition, electronic structure and photoluminescence properties of the nanocrystals⁴¹. In order to minimize this diffusion, the synthesis of the shell must be performed at low temperatures and for a short period of time.

Alternatively, we found that a significant increase of the pho-

toluminescence quantum yield of ZAIS nanocrystals can be obtained when performing a ligand exchange between oleylamine and phosphine-related molecules. It is well known that the choice of capping agent and solvent greatly affects the efficiency of semiconductor nanocrystals⁴². However, to the best of our knowledge, this is the first time that phosphine-related molecules are found to greatly enhance the photoluminescence quantum yield of ternary or quaternary semiconductor nanocrystals. Upon addition of trioctylphosphine, the PLQY of ZAIS nanocrystals synthesized with a precursor composition $X=0.5$ increases from 35% to 49%. The PLQY increases from 48% to 58% for yellow-emitting ($X=0.7$) nanocrystals and from 63% to 78% for red-emitting ($x=0.9$) nanocrystals. This photoluminescence increase is observed for the three contributions and is associated with the increase of their photoluminescence lifetimes. This simultaneous increase of fluorescence lifetimes and quantum yield indicate that this improvement is due to the passivation of non-radiative recombination pathways. Since trioctylphosphine, unlike a ZnS shell, cannot affect the nanocrystals core composition, we can consider this effect to be purely related to surface phenomena. Trioctylphosphine is indeed known to efficiently bond to sulfur surface sites⁴³.

Moreover, as shown in figure 7, the photoluminescence efficiency increase was found to be much larger for the surface contributions ($\sim +110\%$) than for the DAP_{core} contribution ($\sim +35\%$). This confirms our attribution of the recombination processes presented in figure 5. The fact that core emission is also increased via surface passivation can be explained by the diffusion of carriers between the core and the surface of the nanocrystals. The decrease of the total recombination rate on the surface increases the probability that carriers diffuse and relax in the core

of the structure.

Several tests performed with different phosphine-related molecules showed that a better passivation is obtained with molecules that have both an electron-rich phosphorus atom due to electron donating groups and small steric effects to be able to readily adsorb onto the nanocrystals surface. The greatest effect was obtained with tributylphosphine (+ ~ 20%). However, this ligand offers poor stabilization of the nanocrystals in chloroform compared to trioctylphosphine or oleylamine. This limits the practical use of this molecule as a passivating ligand.

When growing a ZnS shell onto ZAIS nanocrystals, the added effect of zinc diffusion can be observed on the emission spectrum of the core contribution. Indeed, the incorporation of zinc into the structure induces an increase of the disorder (E_u) and therefore a decrease of the efficiency. This effect mitigates the benefits of the surface passivation created by the ZnS shell. A combination of ZnS and phosphine passivation can also be used in order to increase even more the global efficiency of the nanocrystals. As an example, the absolute quantum yield of nanocrystals of composition $X=0.7$, emitting in the yellow spectral region, increased from 33% to 50% upon addition of trioctylphosphine. The ZnS shell only increases the quantum yield of these nanocrystals to a value of 42%. The combination on a ZnS shell and trioctylphosphine gives quantum yields of 60%. The same behavior was observed on ZAIS nanocrystals with other compositions ($X=0.4$ and $X=0.9$).

3.5 The effect of surface/volume ratio.

Another direct way to observe the effect of surface on optical properties of ZAIS nanocrystals is to compare nanocrystals of different sizes. Using the alternative synthesis method described in section 2.1, we found that the size of the synthesized nanocrystals increases with the reaction time. On the other hand, the band gap and Urbach energy do not change during the reaction. This indicates that longer reaction times do not affect the composition nor the disorder in the nanocrystals.

Photoluminescence quantum yield measurements performed on ZAIS nanocrystals of different sizes showed that the global photoluminescence quantum yield of ZAIS nanocrystals decreases as their size increases. Moreover, as shown in figure 8, the decrease of PLQY is accompanied by a decrease of the fraction of photons emitted from surface recombinations. Therefore, the global efficiency of ZAIS nanocrystals is controlled by their surface/volume ratio. Higher surface/volume ratios exhibit a larger contribution of the more efficient surface recombination processes thus increasing the overall quantum yield. This effect is however limited by the fact that smaller nanocrystals are not very stable in chloroform. The aggregation of 5.8 nm nanocrystals induce a decrease of the PLQY due to self-quenching of their fluorescence (see figure 8). Nonetheless, these observations are an-

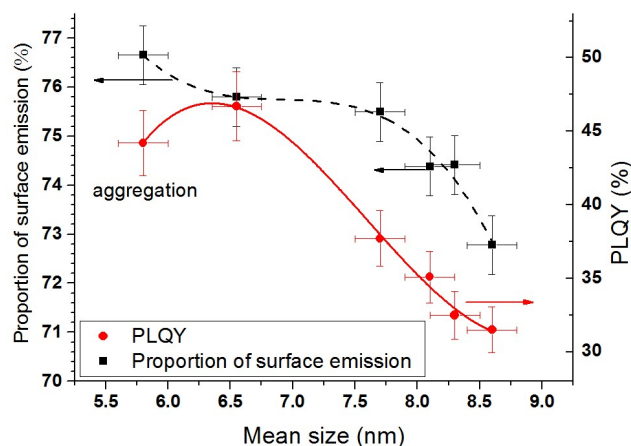


Fig. 8 PLQY and proportion of surface emission as a function of the mean size of ZAIS nanocrystals ($X=0.7$).

other proof of the correct attribution of the different recombination processes to either core or surface phenomena. They are consistent with the fact that highly efficient luminescent quaternary nanocrystals are usually obtained with sizes below 3 nm⁴⁴.

It should be noted that for ultra-small nanocrystals, quantum confinement will eventually modify the electronic states involved in the photoluminescence processes. This effect is already visible for AgInS₂ nanocrystals ($X=1$) since the exciton Bohr radius in this material is estimated to be around 5.5 nm⁴⁵. However, nanocrystals with compositions containing zinc do not exhibit quantum confinement in the range of sizes we tested.

4 Conclusion

The time-resolved emission spectroscopy analysis of AgInS₂-ZnS nanocrystals revealed the existence of three radiative recombinations pathways which could be related to surface and core states. By combining this analysis with photoluminescence quantum yield measurements, we could compare the emission probability of each of the three contributions in nanocrystals of different composition, size and surface chemistry. Radiative recombinations involving surface states appear to be more efficient than those involving core states. Lowering the average size of AgInS₂-ZnS nanocrystals therefore increases their global photoluminescence quantum yield.

A very easy surface passivation method involving the ligand exchange of oleylamine with phosphine-related molecules was developed and showed better results than a ZnS encapsulation. Both these methods act by passivating non-radiative surface defects. They can be used together to give unprecedented quantum yields to AgInS₂-ZnS nanocrystals.

Acknowledgement

The authors would like to thank Professor R. Pansu, S. De Sousa Nobre and F. Agnese for their valuable help on time resolved emission spectroscopy, synthesis and electron microscopy of ZAIS nanocrystals.

References

- H. Duan, Y. Jiang, Y. Zhang, D. Sun, C. Liu, J. Huang, X. Lan, H. Zhou, L. Chen and H. Zhong, *Nanotechnology*, 2013, **24**, 285201.
- B. S. Mashford, M. Stevenson, Z. Popovic, C. Hamilton, Z. Zhou, C. Breen, J. Steckel, V. Bulovic, M. Bawendi, S. Coe-Sullivan and P. T. Kazlas, *Nature Photonics*, 2013, **7**, 407–412.
- P. Mushonga, M. O. Onani, A. M. Madiehe and M. Meyer, *Journal of Nanomaterials*, 2012, **2012**, 1–11.
- D. Aldakov, A. Lefrançois and P. Reiss, *Journal of Materials Chemistry C*, 2013, **1**, 3756.
- I. D. Olekseyuk, V. O. Halka, O. V. Parasyuk and S. V. Voronyuk, *ChemInform*, 2010, **32**, no–no.
- T. Uematsu, T. Doi, T. Torimoto and S. Kuwabata, *The Journal of Physical Chemistry Letters*, 2010, **1**, 3283–3287.
- S. Maeda, T. Uematsu, T. Doi, J. Tokuda, T. Fujita, T. Torimoto and S. Kuwabata, *Electrochemistry*, 2011, **79**, 813–816.
- A. Guchhait and A. J. Pal, *ACS Applied Materials & Interfaces*, 2013, **5**, 4181–4189.
- W. Chung, H. Jung, C. H. Lee and S. H. Kim, *Journal of Materials Chemistry C*, 2014, **2**, 4227–4232.
- S. P. Hong, H. K. Park, J. H. Oh, H. Yang and Y. R. Do, *Journal of Materials Chemistry*, 2012, **22**, 18939.
- P.-J. Wu, K.-L. Ou, J.-K. Chen, H.-P. Fang, S.-H. Tzing, W.-X. Lin and J.-Y. Chang, *Materials Letters*, 2014, **128**, 412–416.
- H. Shinchi, M. Wakao, N. Nagata, M. Sakamoto, E. Mochizuki, T. Uematsu, S. Kuwabata and Y. Suda, *Bioconjugate Chemistry*, 2014, **25**, 286–295.
- P. Zhao, J. Zhang, Y. Zhu, X. Yang, X. Jiang, Y. Yuan, C. Liu and C. Li, *Journal of Materials Chemistry B*, 2014, **2**, 8372–8377.
- D. Deng, J. Cao, L. Qu, S. Achilefu and Y. Gu, *Physical Chemistry Chemical Physics*, 2013, **15**, 5078–5083.
- E. Aazam, *Journal of Industrial and Engineering Chemistry*, 2014, **20**, 4008–4013.
- T. Uematsu, A. Doko, T. Torimoto, K. Oohora, T. Hayashi and S. Kuwabata, *The Journal of Physical Chemistry C*, 2013, **117**, 15667–15676.
- I. Tsuji, H. Kato, H. Kobayashi and A. Kudo, *Journal of the American Chemical Society*, 2004, **126**, 13406–13413.
- E. Sanehira, C.-C. Tu and L. Lin, 2013 Conference on Lasers and Electro-Optics, CLEO 2013, 2013.
- J. Han, Z. Liu, K. Guo, J. Ya, Y. Zhao, X. Zhang, T. Hong and J. Liu, *ACS Applied Materials & Interfaces*, 2014, **6**, 17119–17125.
- T. Torimoto, T. Adachi, K.-i. Okazaki, M. Sakuraoka, T. Shibayama, B. Ohtani, A. Kudo and S. Kuwabata, *Journal of the American Chemical Society*, 2007, **129**, 12388–12389.
- E. Redjai and G. Massâf, *physica status solidi (b)*, 1985, **131**, K157–K159.
- Y. Hamanaka, T. Ogawa, M. Tsuzuki and T. Kuzuya, *The Journal of Physical Chemistry C*, 2011, **115**, 1786–1792.
- Y. Hamanaka, T. Ogawa, M. Tsuzuki, K. Ozawa and T. Kuzuya, *Journal of Luminescence*, 2013, **133**, 121–124.
- T. Torimoto, S. Ogawa, T. Adachi, T. Kameyama, K.-i. Okazaki, T. Shibayama, A. Kudo and S. Kuwabata, *Chemical Communications*, 2010, **46**, 2082.
- B. Mao, C.-H. Chuang, J. Wang and C. Burda, *The Journal of Physical Chemistry C*, 2011, **115**, 8945–8954.
- J. Tauc and A. Menth, *Journal of Non-Crystalline Solids*, 1972, **8-10**, 569–585.
- N. Ghobadi, *International Nano Letters*, 2013, **3**, 2.
- F. Urbach, *Physical Review*, 1953, **92**, 1324–1324.
- S. John, M. Chou, M. Cohen and C. Soukoulis, *Physical Review B*, 1988, **37**, 6963–6976.
- M. Stutzmann, *Philosophical Magazine Part B*, 1989, **60**, 531–546.
- M. Dai, S. Ogawa, T. Kameyama, K.-i. Okazaki, A. Kudo, S. Kuwabata, Y. Tsuboi and T. Torimoto, *Journal of Materials Chemistry*, 2012, **22**, 12851.
- Principles of Fluorescence Spectroscopy*, ed. J. R. Lakowicz, Springer US, Boston, MA, 2006.
- P. R. Bevington, *Data reduction and error analysis for the physical sciences*, McGraw-Hill, Boston, 3rd edn, 2003.
- V. K. Komarala, C. Xie, Y. Wang, J. Xu and M. Xiao, *Journal of Applied Physics*, 2012, **111**, 124314.
- Y. Hamanaka, K. Ozawa and T. Kuzuya, *The Journal of Physical Chemistry C*, 2014, **118**, 14562–14568.
- R. C. Enck and A. Honig, *Physical Review*, 1969, **177**, 1182–1193.
- J. Mooney and P. Kambhampati, *The Journal of Physical Chemistry Letters*, 2013, **4**, 3316–3318.
- S. Ozaki and S. Adachi, *Journal of Applied Physics*, 2006, **100**, 113526.
- S. Ozaki, K.-I. Muto, H. Nagata and S. Adachi, *Journal of Applied Physics*, 2005, **97**, 043507.
- S. Ozaki, S.-i. Boku and S. Adachi, *Physical Review B*, 2003, **68**, 235201.
- B. Mao, C.-H. Chuang, F. Lu, L. Sang, J. Zhu and C. Burda, *The Journal of Physical Chemistry C*, 2013, **117**, 648–656.

- 42 M. M. Krause, J. Mooney and P. Kambhampati, *ACS Nano*, 2013, **7**, 5922–5929.
- 43 K. A. Abel, J. Shan, J.-C. Boyer, F. Harris and F. C. J. M. van Veggel, *Chemistry of Materials*, 2008, **20**, 3794–3796.
- 44 E.-P. Jang, W.-S. Song, K.-H. Lee and H. Yang, *Nanotechnology*, 2013, **24**, 045607.
- 45 Y. J. Park, J. H. Oh, N. S. Han, H. C. Yoon, S. M. Park, Y. R. Do and J. K. Song, *The Journal of Physical Chemistry C*, 2014, **118**, 25677–25683.